UDC: 616.849-051-084:539.16
Professional paper

SPECTRA OF SECONDARY NEUTRONS, ALPHA, BETA AND GAMMA PARTICLES EMERGING ACROSS RADIATION PROTECTION SHIELDING OF A PARTICLE THERAPY CENTER

Mimoza FEJZULLAHI IZAIRI[1], Redona BEXHETI[2], Mimoza RISTOVA[1*]

[1]*Institute of Physics, Department of Faculty of Natural Sciences and Mathematics, University Ss. Cyril and Methodiusin Skopje, MK*
[2]*Department of Faculty of Natural Sciences and Mathematics of the University of Tetova, MK*
[*]*Corresponding author e-mail: mima.ristova@gmail.com*

Abstract

This study presents a comparative analysis of secondary particle spectra emanating from radiation shielding at a particle therapy center. Employing an innovative protective method, concrete-soil sandwich walls with varying soil layer thicknesses (ranging from 150 to 350 cm) were examined for characterization of their shielding capacity. This research was inspired by the shielding design principles of the MedAustron particle therapy facility. Monte Carlo simulations using FLUKA were conducted to model the transport of therapeutic proton or C-ion beams directed at an Average Human Body Phantom (AHUBO), employing 108 primary particles at their maximum therapeutic energies (250 MeV for protons and 430 MeV/u for C-ions), to investigate the secondary fluxes of neutrons, alpha, beta, and gamma particles. The analysis was conducted within a simplified spherical geometry representing the treatment chamber wall, facilitating the respective spectral characteristics. This research contributes to the development of radiation protection methodologies, emphasizing sustainability and performance optimization for future particle therapy centers. By studying the impact of primary particles on parameters such as neutron flux, dose equivalent, neutron spectrum, alpha particles, beta, and gamma particles, the aim is to design a "green" shielding solution tailored to the needs of the International Institute for Sustainable Technologies of Southeast Europe (SEEIIST). Furthermore, the feasibility of utilizing concrete sandwich walls filled with locally excavated soil has been explored to potentially reduce concrete usage and minimize soil removal during foundation laying, thus promoting environmental sustainability.

Keywords: Radiation Protection shielding, Particle therapy centers, Secondary particle spectra, Neutrons, Alpha, Beta Concrete-soil sandwich walls, Monte Carlo simulations, Environmental consciousness

1. Introduction

Particle therapy, employing proton and carbon ion beams, is an innovative cancer treatment approach that precisely targets tumors while sparing surrounding healthy tissues. (Janz, 2004). However, the interaction of these therapeutic beams with shielding materials can lead to the production of secondary particles, such as neutrons and charged particles, establishing unique challenges for radiation protection in particle therapy facilities. (Lindborg, 2013). Effective radiation shielding is essential for ensuring the safety of patients, staff, and the users of the public space around these facilities. While traditional materials like concrete are effective at attenuating radiation, concerns about their environmental impact and secondary radiation production have spurred interest in alternative shielding methods.

Inspired by the advanced design principles of the MedAustron facility, this study explores the efficacy of concrete-soil sandwich walls with varying soil layer thicknesses as a potential "green" shielding solution. Utilizing locally excavated soil reduces reliance on traditional concrete and minimizes environmental disruption associated with soil excavation.

Monte Carlo simulations using FLUKA modify a comprehensive analysis of secondary particle spectra resulting from therapeutic proton or carbon ion beams interacting with the proposed

shielding materials. The study focuses on characterizing neutron, alpha, beta particles and gamma emissions, along with dose equivalent levels within the treatment room environment.
This research aims to advance our understanding of secondary particle production and radiation attenuation in particle therapy facilities, contributing to the development of sustainable and effective radiation protection methodologies. Specifically, the present study seeks to inform the design and implementation of tailored shielding strategies for particle therapy centers in Southeast Europe, supporting initiatives like the International Institute for Sustainable Technologies (SEEIIST). (M.M. Ristova, 2021)(M. Dosanjh, 2022)(U. Amaldi, 2021)
Moreover, investigating concrete-soil sandwich walls not only addresses radiation protection requirements but also aligns with environmental stewardship goals by promoting efficient use of the resources, minimizing the environmental footprint associated with facility construction and later the operation. , while ensuring the safe and effective delivery of advanced particle therapy treatments.
This study aims to analyze secondary particle spectra from radiation shielding in particle therapy centers using simplified spherical geometry. The objectives include assessing the effectiveness of concrete-soil sandwich walls in blocking secondary particles, characterizing the types and amounts of secondary particles produced, optimizing shielding configurations, exploring the use of locally sourced soil in shielding materials, and enhancing understanding of sustainable shielding strategies for improved safety and efficiency in cancer treatment facilities.

2. Methodology

2.1. Monte Carlo simulations: The Monte Carlo (MC) transport code is a method for solving mathematical problems using random sampling, practical to both deterministic (e.g., integral estimation) and stochastic problems (e.g., particle scattering). MC methods are used to resolve stochastic problems, as was established in the 1930s and 1940s (Kalos, 2009). Enrico Fermi (1932) and Stanislaw Ulam with John von Neumann (1947) notably applied MC to calculate neutron diffusion and multiplication (Cooper, 1987)(Islam MR, 2013). FLUKA is a comprehensive Monte Carlo simulation package extensively used in high-energy experimental physics, engineering, shielding, detector and telescope design, cosmic ray studies, dosimetry, medical physics, and radiobiology (Battistoni, 2007). It is an indispensable tool for accelerator shielding and target design to cosmic rays, radiotherapy, and more (Fasso, 2003). Monte Carlo is often likened to a "mathematical experiment," where results, of the simulation outcomes are called estimators, akin to real experimental measurements with statistical and systematic errors (De Saint-Hubert, 2022).
Our simulations apply USRBDX to score double-differential fluence (Φ) or current from energy (-log E) and solid angle (Σ) on specific interfaces (boundary surfaces), while USRBIN records spatial energy distribution or total fluence within a mesh of nods defined by the user in cylindrical or Cartesian geometry.

2.2. AHUBO phantom: For this study, we formed an atomic stoichiometry model of a human body phantom (AHUBO), comprising a homogeneous mixture of elements with a mass content precision of better than 0.2% (R.I.-Bexheti M. R., 2023). The model assumes the average human body composition includes: $O_{24}C_{12}H_{62}N_{1.1}Ca_{0.22}P_{0.22}$ (Anne Marie, 2020), used density 0.986 g/cm^3.

2.3. A spherical model of sandwich walls: The MC FLUKA simulations aimed to compare secondary particle fluences of neutrons, alpha, beta, and gamma particles — produced by 10^8

primary protons at 250 MeV or primary carbon ions at 430 MeV/u, both used in particle therapy (Izairi-Bexheti, 2023). This study focused on evaluating the effectiveness of the Concrete-Soil-Concrete (CSC) shielding approach for radiation protection in particle therapy centers. The analysis focused on assessing how changes in the soil layers of this configuration impact shielding effectiveness while maintaining identical spherical geometry (Figure 1). The overall setup consists of a spherical shell of 30 cm thick reinforced concrete walls with soil in between. Between these walls there is soil layer with variable thickness ranging from 150 cm to 350 cm around the head model (AHUBO sphere of 8 cm radius). The distance from the AHUBO phantom (P) to the configuration (CNC shield) is 200 cm. For the concrete wall shielding material, we have considered Portland-type of concrete, commonly used, with density 2.350 g/cm^3, which has a stoichiometry already in place with the FLUKA program's database: $C_{23}O_{40}Si_{12}Ca_{12}H_{10}Mg_2$. The soil used to simulate the filling between the concrete CSC walls was sampled from the potential site of SEEIIST located in the Skopje region of North Macedonia. Its stoichiometry has been previously evaluated through energy dispersion X-ray analysis by scanning electron microscopy with energy dispersion od X-rays spectroscopy (SEM/EDX) to be $A_{3.71}C_{8.89}Ca_{5.53}Fe_{5.26}Mg_{4.05}O_{56.36}Si_{16.18}$ (Izairi-Bexheti R. R., 2023, Submitted for publication).The particle density of the soil was assumed to be the density of an average soil, 1.5 g/cm^3 (Blake, 1986).

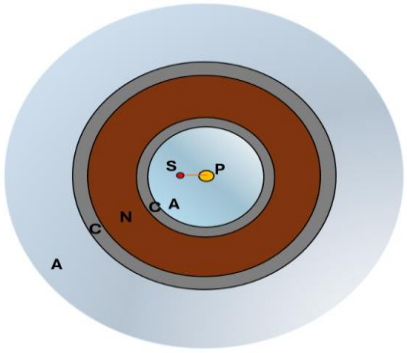

Figure 117. An illustration of the problem geometry, depicting a spherical shield configuration denoted as concrete-soil sandwich configuration, where N represents soil within the CSC setup. S denotes the ion/proton source, and P stands for the AHUBO phantom. The blue region signifies air (A).

2.4. Secondary particles production : Secondary particles, including neutrons, alpha particles, beta particles, and gamma photons, are produced because of interactions between primary particles (such as protons or heavy ions) and matter. Here's an overview of how these secondary particles are generated:

- **Neutrons:** Neutrons are commonly produced through nuclear reactions involving the collision of primary particles (like protons or heavy ions) with atomic nuclei within the target material. These reactions include nuclear spallation, where a nucleus is fragmented into smaller particles, including neutrons, or nuclear fission, where a nucleus splits into smaller fragments along with the release of several neutrons to pursue a chain reaction.
- **Alpha Particles:** Alpha particles are helium nuclei consisting of two protons and two neutrons. They can be produced through nuclear reactions where a heavy ion (such as a proton or carbon ion) interacts with a target nucleus, leading to the emission of an alpha particles as a product of certain nuclear reactions.
- **Beta Particles:** Beta particles can be either electrons (beta-minus) or positrons (beta-plus). They are produced primarily through beta decay processes of unstable atomic nuclei. In particle therapy, beta particles may be generated as secondary particle from the interaction of the primaries with target materials, forming beta-emitting isotopes thereby.

- **Gamma Particles (Gamma Rays):** Gamma rays are high-energy electromagnetic radiation emitted from atomic nuclei following nuclear reactions or radioactive decay processes. In the context of particle therapy, gamma rays can be produced as secondary radiation when high-energy primary particles interact with matter, leading to nuclear transitions within the atomic nuclei (metastabile to stabile), resulting in gamma-ray emission.

The production of these secondary particles depends on factors like the energy and type of primary particles, properties of the target material, and the nature of nuclear interactions involved. Understanding their production and behavior is crucial for assessing radiation dose distribution and designing effective shielding strategies in particle therapy and other radiation-related applications. Characterizing the spectra of secondary particles in terms of fluence or its double differential as a function of energy is an important aspect addressed by Monte Carlo (MC) simulation tools. The latter findings could serve to create an optimized environmentally friendly and sustainable shielding design.

3. Results and discussion

3.1. Simulation with primary protons of 250 MeV:

3.1.1. Secondary particles: Neutrons: Figure 2182 displays the results concerning secondary neutrons. These simulations employed the USRBDX function within FLUKA, triggered by 10^8 primary protons of 250 MeV directed towards the center of the head of the AHUBO phantom. The 2D fluency distributions are depicted for (a) a soil thickness of 150 cm and (b) a soil thickness of 350 cm within the Concrete – Soil - Concrete configuration. A noticeable decrease in the flow of secondary neutrons is evident as the soil thickness increases in the configuration.

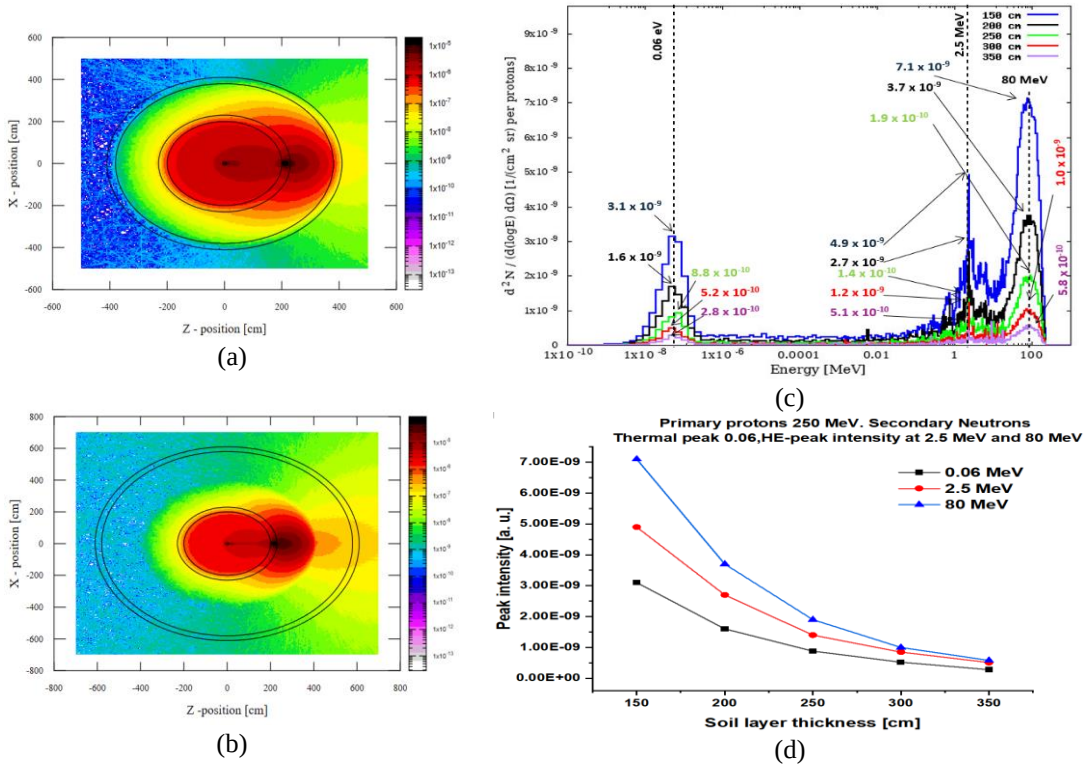

Figure 218. 2D fluence of secondary neutrons for concrete walls shielding with in between: (a) 150 cm thick layer of soil, (b) 350 cm thick soil, and (c) illustrates the double differentials of neutron fluence as a function of energy when soil thickness changes in the CNC configuration during irradiation of the AHUBO phantom with 108 primary protons at 250 MeV, (d) decrease of thermal peak at 0,06 eV, HE peaks at 0.5 and 2.1 MeV with shielding soil thickness.

Panel (c) illustrates the double differentials of neutron fluence concerning energy variations when soil thickness changes in the concrete-soil sandwich configuration. The spectrum of secondary neutrons manifests two energy maxima regions. In the thermal region, with neutrons at an energy of 0.06 eV, the intensity reduces from 3.1×10^{-9} to 2.8×10^{-10} (about one order of magnitude) In the high energy region, there are two peaks, at 2.5 MeV and 80 MeV. The intensity of the latter drops from 7.1×10^{-9} to 5.8×10^{-10}. The protective capacity of the soil layer and the impact of its thickness is evident as a for shielding material in secondary neutron production. Figure 2 (d) clearly shows that thermal peak at 0.06 eV and both the HE peaks (at 2.5 and 80 MeV decline with the soil layer thickness). The declination however demonstrates tendency of saturation at 350 cm thickness, suggesting that no further increase of the soil layer would be justified for gamma dose reduction under the afore mentioned conditions.

3.1.2. Secondary particles: Alphas:

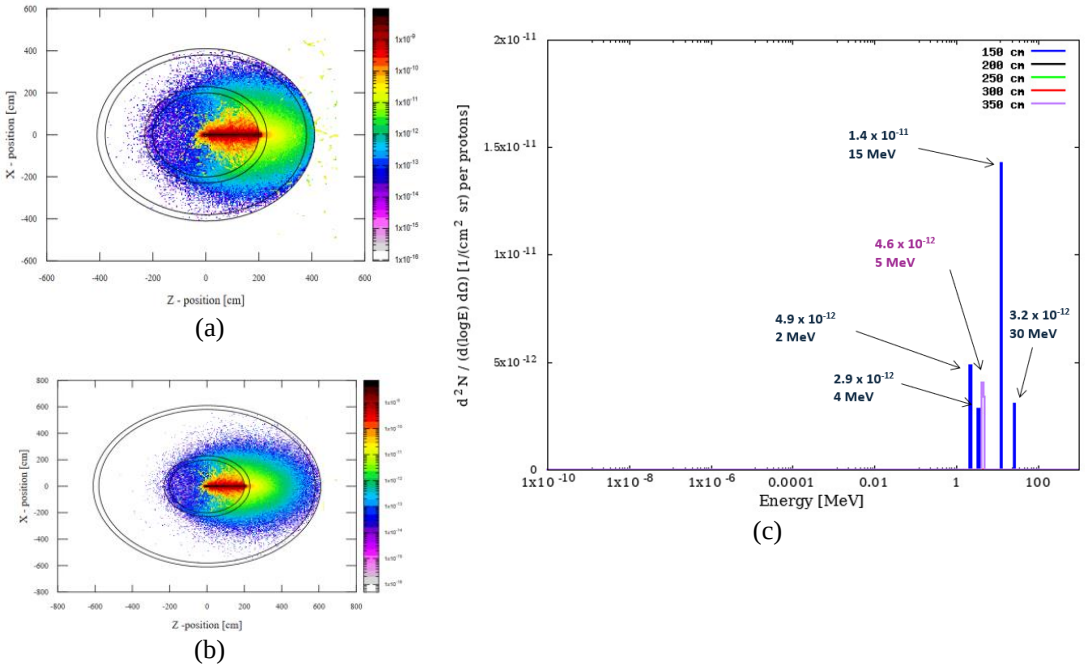

Figure 3. 2D fluence secondary alpha particle results: (a) 150 cm soil thickness, (b) 350 cm soil thickness, and (c) illustrates the double differentials of alpha particle fluence as a function of energy when soil thickness changes in the soil-concrete sandwich configuration from 150-350 cm, with step 50 cm, during irradiation of the AHUBO phantom with 10^8 primary protons at 250 MeV

Figure3 presents the results related to secondary alpha particles. These simulations utilized the USRBDX function within FLUKA, initiated by 10^8 primary protons of 250 MeV directed towards the center of the head of the AHUBO-n phantom. The 2D fluence distributions are showcased for (a) a soil thickness of 150 cm and (b) a soil thickness of 350 cm within the soil-concrete sandwich configuration. A noticeable decline in the flux of secondary alpha particles is observable as the soil thickness increases in the configuration. Herein, panel (c) shows the double differentials of secondary alpha particle fluence concerning energy variations when soil thickness varies in the examined shielding configuration. The spectrum of secondary alpha particles exhibits only a handful of discrete lines. At an energy of 15 MeV, the intensity is 1.4×10^{-11}, while for spectral line at 5 MeV, the intensity is 4.6×10^{-12}.

3.1.3. Secondary particles: Beta: Figure 4 displays the results concerning secondary beta particles. These simulations work the USRBDX function within FLUKA, triggered by 108 primary protons of 250 MeV directed towards the center of the head of the AHUBO-n phantom.

The 2D fluence distributions are depicted for (a) a soil thickness of 150 cm and (b) a soil thickness of 350 cm within the – concrete - soil sandwich configuration. A notable decrease in the fluence of secondary beta particles is evident as the soil thickness increases in the shielding sandwich configuration.

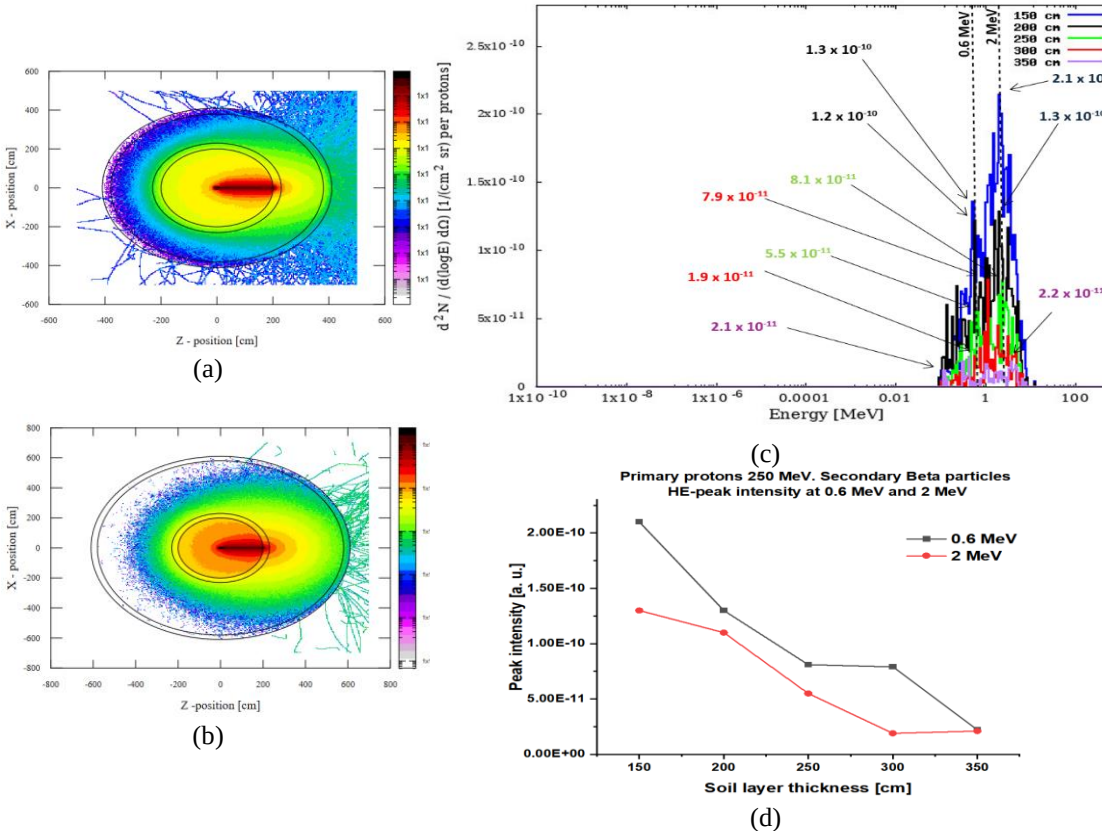

Figure 4. 2D fluence of secondary beta particle results: (a) 150 cm soil thickness, (b) 350 cm soil thickness, and (c) illustrates the double differentials of beta particle fluence as a function of energy for soil thickness changes from 150-350 cm, with step 50 cm) in the sandwich shielding configuration during irradiation of the AHUBO phantom with 10^8 primary protons at 250 MeV, (d) decrease of HE peaks at 0.5 and 2.1 MeV with shielding soil thickness.

Panel (c) illustrates the double differentials of beta particle fluence concerning energy variations when soil thickness changes in the CNC configuration. The spectrum of secondary beta particles manifests two energy maxima regions. In the high energy region, at 0.6 MeV and 2 MeV, the intensity reduces from 2.1×10−10to 2.2×10−11. The variations in soil thickness demonstrate marked impacts on beta particle fluence and energy spectrum, underscoring the significance of shielding material in secondary beta particle production. Figure 4 (d) clearly shows both the HE peaks (at 0,6 and 2 MeV decline with the soil layer thickness). The declination however demonstrates a tendency of saturation at 350 cm thickness, suggesting that no further increase of the soil layer would be justified for gamma dose reduction under the aforementioned conditions.

3.1.4. Secondary particles: Gamma: Figure 5 displays the results concerning secondary gamma particles. These simulations employed the USRBDX function within FLUKA, triggered by 108 primary protons of 250 MeV directed toward the center of the head of the AHUBO-n phantom. The 2D fluence distributions are depicted for (a) a soil thickness of 150 cm and (b) a soil thickness of 350 cm within the Concrete – Soil - Concrete configuration. An obvious decrease in the fluence of secondary gamma photons is evident as the soil thickness increases in the

shielding configuration. Panel (c) illustrates the double differentials of gamma particle fluence concerning energy variations when soil thickness changes in the shielding configuration.

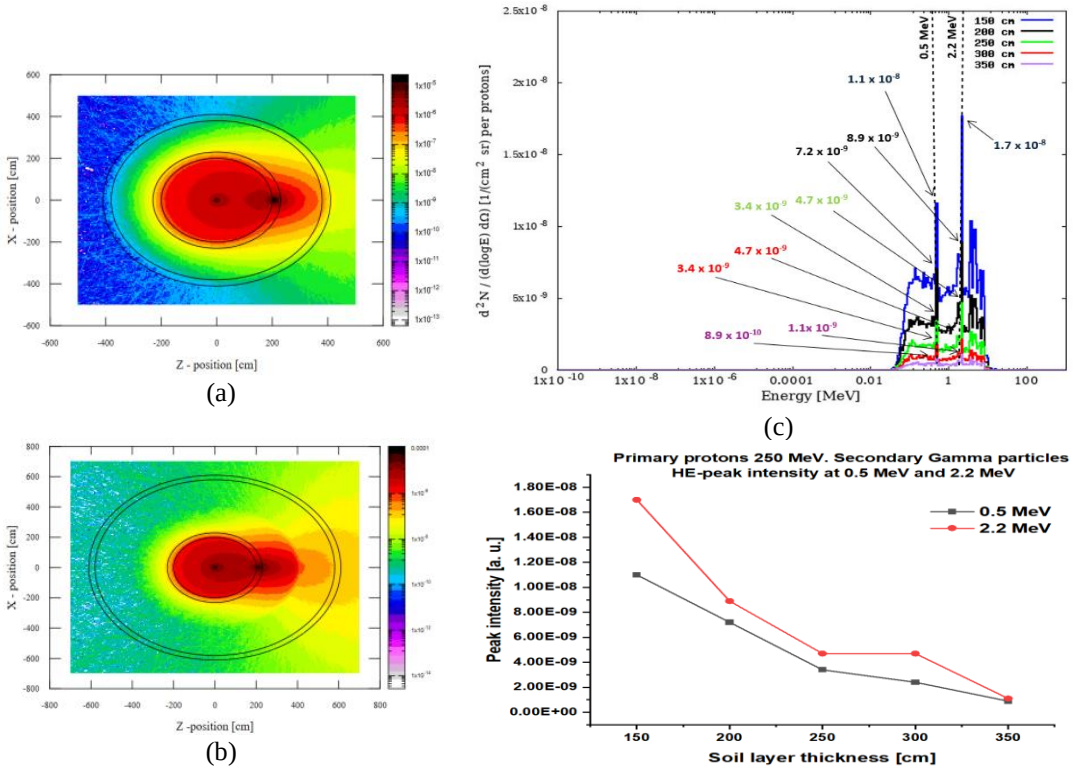

Figure 5. 2D fluence secondary gamma particle results: (a) 150 cm soil thickness, (b) 350 cm soil thickness, and (c) spectral distribution - double differentials of gamma particle fluence as a function of energy when soil thickness changes in the shielding configuration from 150-350 cm, with step 50 cm, during irradiation of the AHUBO phantom with 10^8 primary protons at 250 MeV, (d) decrease of HE peaks at 0.5 and 2.2 MeV with shielding soil thickness.

As evident from Figure 5. (c) the spectrum of secondary gammas reveals two high-energy maxima at 0.5 MeV and 2.2 MeV. Their intensity falls from 1.7×10−8 to 1.1×10−9 for the increased thickness of the soil layer. Figure 5 (d) clearly shows both the HE peaks (at 0.5 and 2.2 MeV decline with the soil layer thickness). The declination however demonstrates a tendency of saturation at 350 cm thickness, suggesting that no further increase of the soil layer would be justified for gamma dose reduction under the aforementioned conditions.

3.2. Simulation with primary C-ions of 430 MeV/u :

*3.2.1. Secondary particles: Neutrons:*Figure **619**6 displays the results concerning secondary neutrons. These simulations employed the USRBDX function within FLUKA, triggered by 10^8 primary C-ions of 430 MeV/u directed towards the center of the head of the AHUBO-n phantom. The 2D fluence distributions are depicted for (a) a soil thickness of 150 cm and (b) a soil thickness of 350 cm within the Concrete – Soil - Concrete configuration. A noticeable decrease in the flow of secondary neutrons is evident as the soil thickness increases in the configuration.

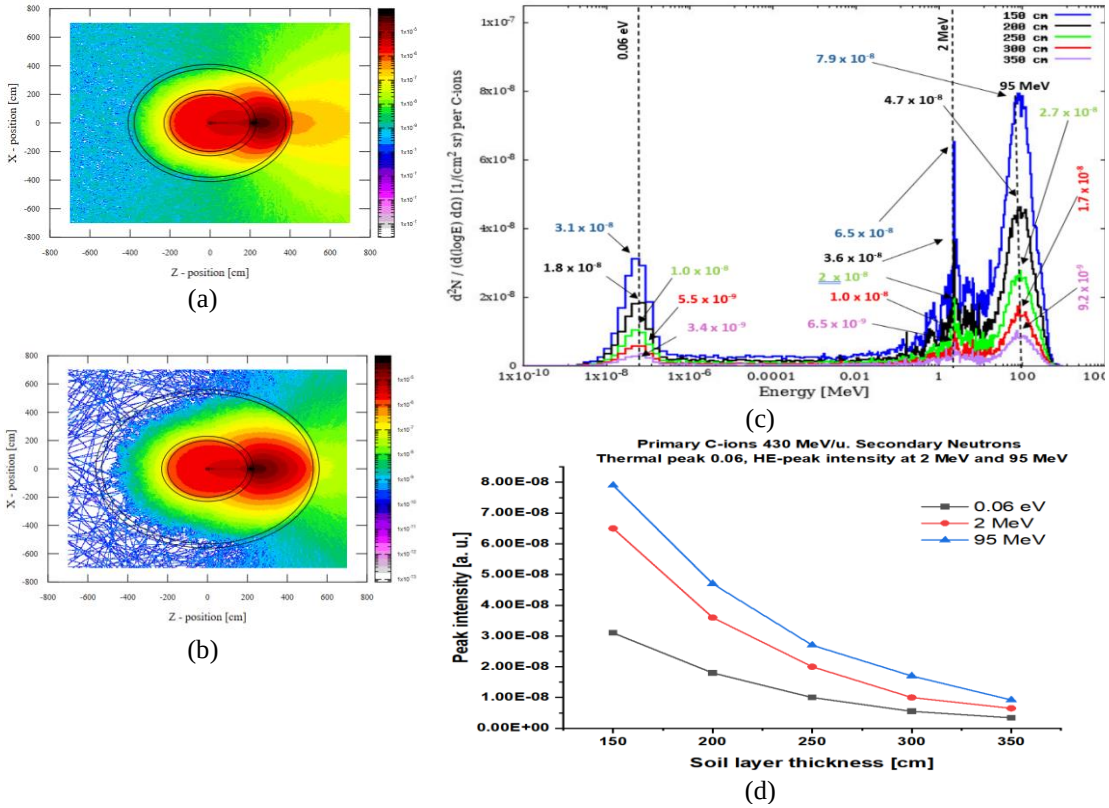

Figure 619. 2D fluence secondary neutrons for concrete walls shielding with in between: (a) 150 cm thick layer of soil, (b) 350 cm thick soil, and (c) illustrates the double differentials of neutron fluence as a function of energy when soil thickness changes in the CNC configuration during irradiation of the AHUBO phantom with 10^8 primary C-ions at 430 MeV/u (d) decrease of thermal peak at 0,06eV and HE peaks at 0.5 and 2.2 MeV with shielding soil thickness.

Panel (c) illustrates the double differentials of neutron fluence concerning energy variations when soil thickness changes in the concrete-soil sandwich configuration. The spectrum of secondary neutrons manifests two energy maxima regions. In the thermal region, with neutrons at an energy of 0.06 eV, the intensity reduces from 3.1×10−8 to 3.4×10−9(about one order of magnitude) In the high energy region, there are two peaks, at 2 MeV and 95 MeV. The intensity of the latter drops from 7.9×10−8 to 9.2×10−9. The protective capacity of the soil layer and the impact of its thickness is evident as a shielding material in secondary neutron production. Figure 6 (d) clearly shows a thermal peak at 0,06 eV and both the HE peaks (at 0.5 and 2.2 MeV decline with the soil layer thickness). The declination however demonstrates a tendency of saturation at 350 cm thickness, suggesting that no further increase of the soil layer would be justified for gamma dose reduction under the aforementioned conditions.

3.2.2. Secondary particles: Alphas

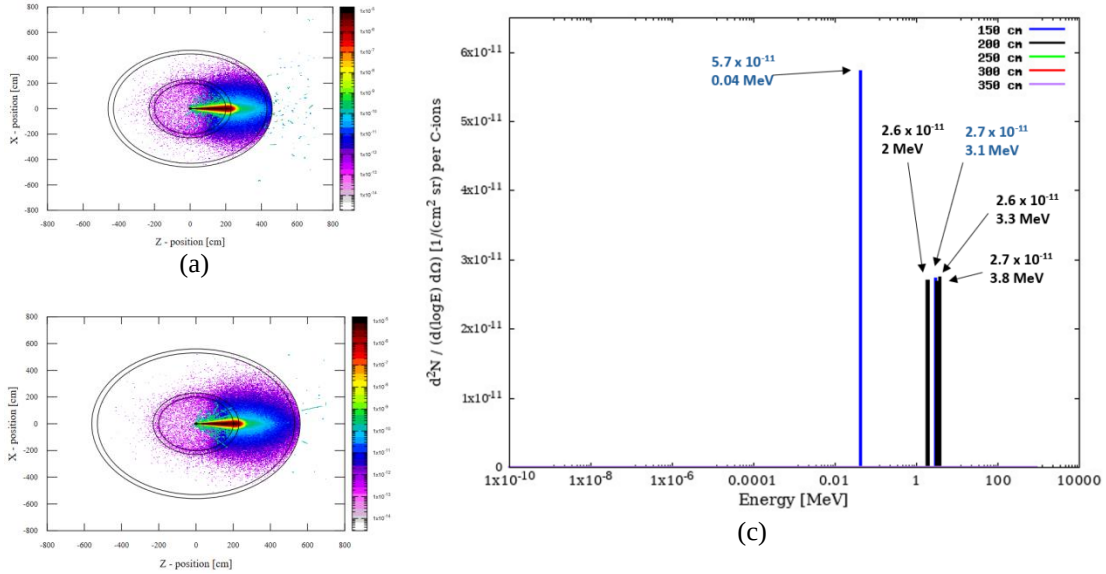

Figure 720. 2D fluence secondary alpha particle results: (a) 150 cm soil thickness, (b) 350 cm soil thickness, and (c) illustrates the double differentials of alpha particle fluence as a function of energy when soil thickness changes in the soil-concrete sandwich configuration from 150-350 cm, with step 50 cm, during irradiation of the AHUBO phantom with 10^8 primary C-ions at 430

Figure **720**7 presents the results related to secondary alpha particles. These simulations utilized the USRBDX function within FLUKA, initiated by 10^8 primary C-ions of 430 MeV/u directed towards the center of the head of the AHUBO-n phantom. The 2D fluence distributions are showcased for (a) a soil thickness of 150 cm and (b) a soil thickness of 350 cm within the soil-concrete sandwich configuration. A noticeable decline in the flux of secondary alpha particles is observable as the soil thickness increases in the configuration. Herein, panel (c) shows the double differentials of secondary alpha particle fluence concerning energy variations when soil thickness varies in the examined shielding configuration. The spectrum of secondary alpha particles exhibits only a handful of discrete lines. At an energy of 0.04 MeV, the intensity registers at 5.7 $\times 10^{-11}$, while for spectra with 3.3 MeV, the intensity is 2.7×10^{-11}.

3.2.3. Secondary particles: Beta: Figure **821**8 displays the results concerning secondary beta particles. These simulations employed the USRBDX function within FLUKA, triggered by 10^8 primary C-ions of 430 MeV/u directed towards the center of the head of the AHUBO-n phantom. The 2D fluence distributions are depicted for (a) a soil thickness of 150 cm and (b) a soil thickness of 350 cm within the –concrete-soil sandwich configuration. A notable decrease in the fluence of secondary beta particles is evident as the soil thickness increases in the shielding sandwich configuration.

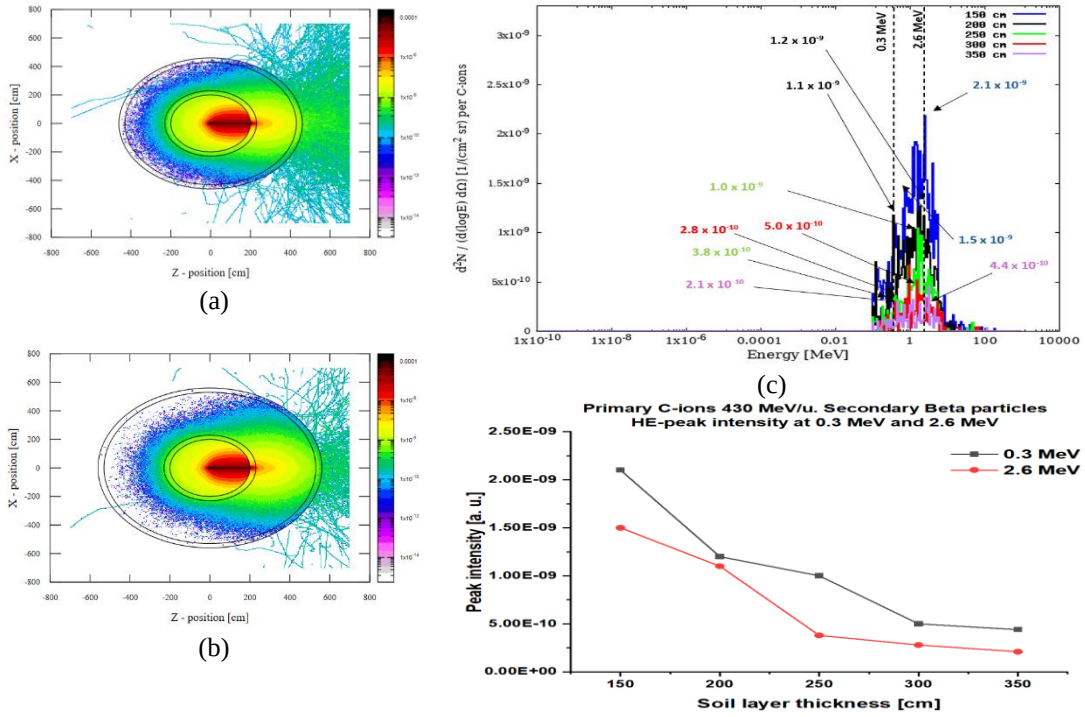

Figure 821. 2D fluence of secondary beta particle results: (a) 150 cm soil thickness, (b) 350 cm soil thickness, and (c) illustrates the double differentials of beta particle fluence as a function of energy for soil thickness changes from 150-350 cm, with step 50 cm) in the sandwich shielding configuration during irradiation of the AHUBO phantom with 10^8 primary C-ions at 430 MeV/u (d) decrease of HE peaks at 0.3 and 2.6 MeV with shielding soil thickness.

Panel (c) illustrates the double differentials of beta particle fluence concerning energy variations when soil thickness changes in the CNC configuration. The spectrum of secondary beta particle manifests two energy maxima regions. In the high energy region, at 0.3 MeV, and 2.6 MeV, the intensity reduces from 2.1×10^{-9} to 4.4×10^{-10}. The variations in soil thickness demonstrate marked impacts on beta particles fluence and energy spectrum, underscoring the significance of shielding material in secondary beta particles production. Figure 8 (d) clearly shows the HE peaks (at 0.3 and 2.6 MeV decline with the soil layer thickness). The declination however demonstrates tendency of saturation at 350 cm thickness, suggesting that no further increase of the soil layer would be justified for gamma dose reduction under the afore mentioned conditions.

3.2.4. Secondary particles: Gamma: Figure8 displays the results concerning secondary gamma particles. These simulations employed the USRBDX function within FLUKA, triggered by 10^8 primary C-ions of 430 MeV/u directed towards the center of the head of the AHUBO-n phantom. The 2D fluence distributions are depicted for (a) a soil thickness of 150 cm and (b) a soil thickness of 350 cm within the Concrete – Soil - Concrete configuration. An obvious decrease in the fluence of secondary gamma photons is evident as the soil thickness increases in the shielding configuration. Panel (c) illustrates the double differentials of gamma particle fluence concerning energy variations when soil thickness changes in the shielding configuration.

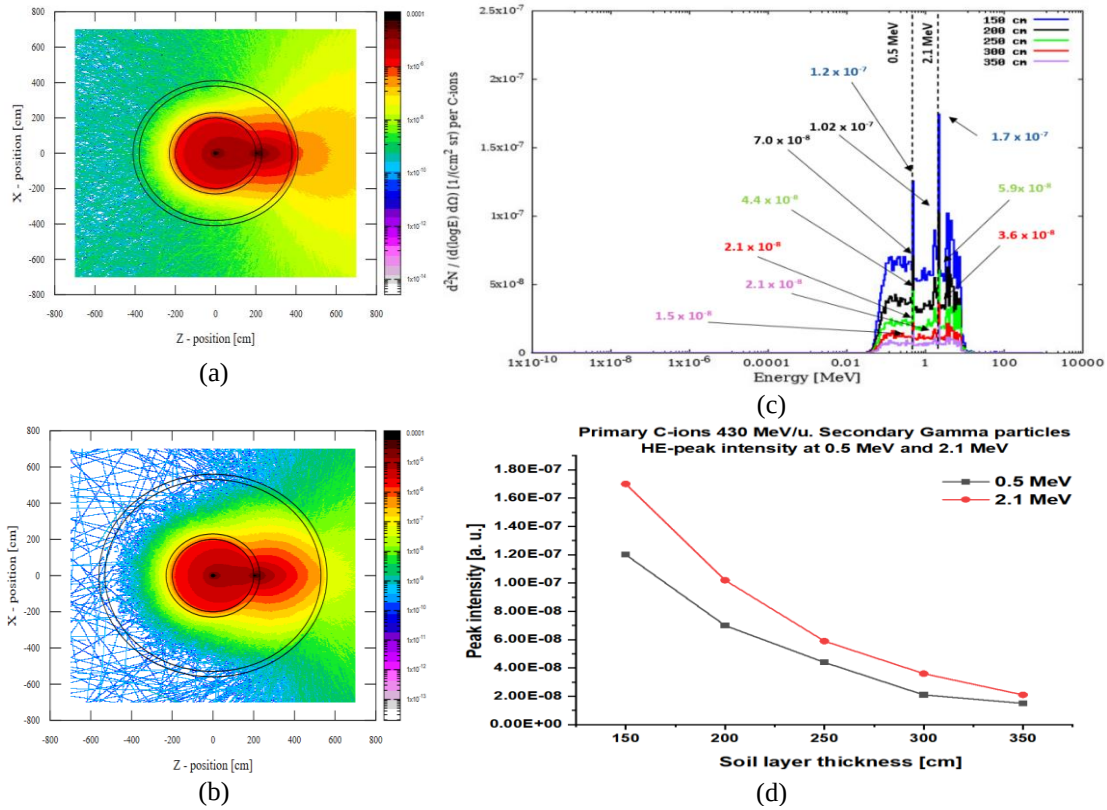

Figure 8. 2D fluence secondary gamma particle results: (a) 150 cm soil thickness, (b) 350 cm soil thickness, and (c) illustrates the double differentials of gamma particle fluence as a function of energy when soil thickness changes in the CNC configuration during irradiation of the AHUBO phantom with 10^8 primary C-ions at 430 MeV/u, (d) decrease of HE peaks at 0.5 and 2.1 MeV with shielding soil thickness.

The spectrum of secondary gamma particles manifests two high energy maxima. In the high energy region, at 0.5 MeV and 2.1 MeV, the intensity reduces from 1.7×10^{-7} to 2.1×10^{-8}. The variations in soil thickness demonstrates visible impact on gamma fluence and energy spectrum. Figure 9 (d) clearly shows that both the HE peaks (at 0.5 and 2.1 decrease with the soil layer thickness). The declination however demonstrates tendency of saturation at 350 cm thickness, suggesting that no further increase of the soil layer would be justified for gamma dose reduction under the afore mentioned conditions.

4. Conclusions

Through extended Monte Carlo (MC) simulations using FLUKA, we have evaluated the effectiveness of Concrete-Soil-Concrete (CSC) shielding for particle therapy centers. This study compared secondary particle spectra produced by 10^8 primary protons at 250 MeV or primary carbon ions at 430 MeV/u, commonly used in particle therapy. Our analysis focused on varying soil layer thicknesses while maintaining identical spherical geometries around an AHUBO phantom with an 8 cm radius. The results demonstrate that the CSC shielding configuration effectively attenuates secondary particle streams, including neutrons, alpha particles, beta particles, and gamma rays, emitted by therapeutic proton and carbon ion beams.

This study has shown that, as expected, the thicker the soil layer within the concrete-soil sandwich shielding configuration, the particles of interest are shielded. However, limitations arose from the absence of experimental equipment to directly validate our simulations against real-world measurements using detectors targeting an AHUBO phantom. Future simulations should consider using a larger number of primary particles (e.g., 10^{10}) to improve statistical accuracy and validate practical applicability.

In conclusion, this study highlights the importance of rigorous Monte Carlo simulations in developing optimized radiation protection strategies for particle therapy centers. The findings contribute to enhancing safety and efficiency in cancer treatment facilities. Integrating experimental validation and larger-scale simulations will advance our understanding and implementation of effective radiation protection methodologies in particle therapy and related medical applications.

Recommendation

The study's limitations stem from the absence of experimental equipment capable of directing accelerated primary particles (protons and carbon ions) used in particle therapy toward a real AHUBO phantom. This impedes direct comparison between our Monte Carlo simulation outcomes and experimental results obtained using actual detectors. To address this, future simulations should consider using a larger number of primaries, ideally around 10^{10}.

References

[1] Anne Marie. (2020, October 29). What Are the Elements in the Human Body?

[2] Battistoni, G. a. (2007). The FLUKA code: Description and benchmarking. *AIP Conference proceedings, 896*, 31--49.

[3] Chetty, I. J.-M. (2007). Report of the AAPM Task Group No. 105: Issues associated with clinical implementation of Monte Carlo-based photon and electron external beam treatment planning. *Medical physics, 34*(12), 4818--4853.

[4] Cooper, N. (1987). *os Alamos Science Number 15: Special Issue on Stanislaw Ulam 1909-1984*. Los Alamos National Lab.(LANL), Los Alamos, NM (United States).

[5] De Saint-Hubert, M. a.-E. (2022). The influence of nuclear models and Monte Carlo radiation transport codes on stray neutron dose estimations in proton therapy. *Radiation Measurements* (150), 106693.

[6] Fasso, A. a. (2003). The physics models of FLUKA: status and recent development. *arXiv preprint hep-ph/0306267*.

[7] Islam MR, C. T. (2013). Off-axis dose equivalent due to secondary neutrons from uniform scanning proton beams during proton radiotherapy. *Physics in Medicine \& Biology, 58*(22), 8235.

[8] Izairi-Bexheti., R. M. (2023). Angular distribution of neutrons from proton and carbon ion therapy using AHUBO phantom (Monte Carlo simulations with Fluka). *ACTA MEDICA BALCANICA, 8*(15-16), 294 - 304.

[9] Janz, N. K. (2004). Patient-physician concordance: preferences, perceptions, and factors influencing the breast cancer surgical decision. *Journal of clinical oncology, 22*(15), 3091-3098.

[10] Kalos, M. H. (2009). *Monte carlo methods*. John Wiley \& Sons.

[11] Lindborg, L. a. (2013). Lineal energy and radiation quality in radiation therapy: model calculations and comparison with experiment. *Physics in medicine \& Biology, 58*(10), 3089.

[12] M. Dosanjh, R. M. (2022). Availability of technology for managing cancer patients in the Southeast European (SEE) region. *Clinical and Translational Radiation Oncology, 34*, 57--66.

[13] M.M. Ristova, V. G. (2021). Patients with cancer in the countries of south-east europe (the Balkans) region and prospective of the particle therapy center: South-East European International Institute for Sustainable Technologies (SEEIIST). *Advances in Radiation Oncology, 6*(6), 100772.

[14] R.I.-Bexheti, M. R. (2023). Applited Radiation and Isotops, Submitted for publication.

[15] U. Amaldi, E. B. (2021). South East European International Institute for Sustainable Technologies (SEEIIST). *Frontiers in Physics, 8*, 567466.